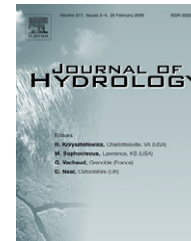




available at www.sciencedirect.com



journal homepage: www.elsevier.com/locate/jhydrol



Three-dimensional effects causing artifacts in two-dimensional, cross-borehole, electrical imaging

Robin E. Nimmer ^{a,*}, James L. Osiensky ^a, Andrew M. Binley ^b
Barbara C. Williams ^c

^a *University of Idaho, Department of Geological Sciences, P.O. Box 443022, Moscow, ID 83844-3022, USA*

^b *Lancaster University, Lancaster Environment Centre, Lancaster LA1 4YQ, United Kingdom*

^c *University of Idaho, Department of Biological and Agricultural Engineering, P.O. Box 440904, Moscow, ID 83844-0904, USA*

Received 1 November 2007; received in revised form 2 May 2008; accepted 7 June 2008

KEYWORDS

Electrical resistance tomography;
Borehole inversion effects;
Shadow effects;
Numerical modeling

Summary Cross-borehole electrical resistance tomography (ERT) experiments utilize downhole electrodes, typically placed in a borehole filled with material of contrasting resistivity to the host rock. The circular geometry of the boreholes is three-dimensional, and inversion routines are typically two-dimensional. Because of the resistivity contrast, artifacts in the form of borehole inversion effects develop in the resistivity images. Other 3D effects resulting in inversion artifacts are shadow effects caused by use of a 2D code to invert data from a 3D body located outside the image plane. In both cases the inversion model misrepresents the spatial change in voltages as a corresponding spatial change in resistivity. Borehole inversion effects and shadow effects result as the forward solver attempts to resolve the discrepancy in the voltages for numerous electrode pairs into a meaningful resistivity distribution. Borehole inversion effects are shown to be related to the resistivity contrast between the borehole fill and the host medium, and to borehole diameter.

Borehole inversion effects do not materialize with small diameter boreholes (e.g. ≤ 0.1 m) when the fill resistivity contrast is one order of magnitude or less; however, a borehole fill resistivity contrast of two orders of magnitude causes artifacts in the form of sheaths near the boreholes, and a conductive artifact between the boreholes. Larger diameter borehole (e.g. 0.2 m) induce significant borehole inversion effects with as little as one order of magnitude fill resistivity contrast. The general resistivity patterns are similar for the borehole inversion effects. However, the artifacts are amplified as resistivity

* Corresponding author. Tel.: +1 208 301 2078; fax: +1 208 885 7908.

E-mail addresses: nimmer@uidaho.edu (R.E. Nimmer), osiensky@uidaho.edu (J.L. Osiensky), a.binley@lancaster.ac.uk (A.M. Binley), barbwill@uidaho.edu (B.C. Williams).

contrast and/or borehole diameter increase. These results are significant because borehole inversion effects may mask a target heterogeneity or an artifact may be confused for an anomaly resulting in improper actions for site characterizations or remediation strategies. Suggestions of best practices for experimental design to prevent or minimize borehole inversion effects include: minimizing borehole diameter, minimizing borehole fill resistivity contrast, measuring and inputting the resistivity of the borehole fill/water into the model, and inverting changes in resistivity for time-lapse ERT data.

Shadow effects are shown to be related directly to the distance of the target heterogeneity out of the image plane. Our results show that shadow effects become insignificant when the target is between 3 and 5 m outside the 10-m wide image plane. Because the size of the target and resistivity contrast of the target to the host rock are site-specific variables, the actual distance at which shadow effects become insignificant will vary from site to site. To reduce misinterpretations by shadow effects reduce the dipole length of the four electrode measurements and supplement data from other well pairs and/or other methods.

Published by Elsevier B.V.

Introduction

Statement of the problem

Cross-borehole electrical resistance tomography (ERT) is a useful tool to monitor subsurface hydrological and remediation processes (e.g. LaBrecque et al., 1996). However, two common occurrences related to the collection and inversion of cross-borehole ERT data can lead to erroneous interpretations. Typically, the subsurface resistivity distribution between two wells is estimated using an inversion code based on 3D current flow but only 2D resistivity distribution (this is usually referred to as 2.5D inversion). Use of a 2.5D code where 3D structures prevail (e.g. boreholes and contaminant plumes) may result in image artifacts. The second ERT limitation is a weak sensitivity in the center volume between the columns of electrodes (boreholes). Image resolution is poor in the center volume relative to the areas near the electrodes, as shown by Day-Lewis et al. (2005).

One type of 3D effect results from the cylindrically-shaped discontinuities formed by boreholes (Osiensky et al., 2004). In most cases, the only access to the subsurface for placement of electrodes is through boreholes. The 3D nature of the borehole itself presents an issue when using a 2.5D inversion model to interpret the data. Furthermore, electrodes generally must be positioned below the water table, or in a backfilled portion of the borehole, or another form of coupling mechanism must be used (e.g. flexible tubular liners to press a string of electrodes against the borehole walls) to create reliable, electrical contact with the host material. Often determination of the resistivity contrast between the borehole fill and host material is not as high a priority as maintaining good, reliable, electrical continuity with the borehole walls. In addition, the actual resistivity of the fill may not be known or may change over time. Even with detailed knowledge of the electrical properties of the fill material, incorporation of this information into the inversion procedure would necessitate the use of a 3D forward model within the inversion routine. If the resistivity contrast of the borehole fill, and the volume of the borehole are disregarded, the 2.5D inversion code generates spatial image artifacts as part of a numerical solution to a

technically ill-defined problem. These borehole inversion effects may develop from a combination of factors including irregular current flow near an irregularly shaped borehole, cylindrical current flow through the borehole fill, heterogeneity of the borehole fill, poor electrical continuity between electrodes and borehole walls, and/or 3D/2D model treatment of boreholes as absent or as element shaped prisms. Borehole inversion effects often are included under the category of noise. Other forms of noise result from poor electrode coupling with the host rock, random errors associated with the transmitter/receiver, and errors caused by extraneous effects (Slater et al., 2000).

Indurated rock, such as limestone, quartzite, lavas, granite or gneisses, may have resistivities as much as three orders of magnitude greater than nonindurated materials (Keller and Frischknecht, 1966; Telford et al., 1990; Parkhomenko, 1967; Bear et al., 1993), thereby creating a significant resistivity contrast with a backfilled borehole or a borehole filled with water. Most backfill materials and water have lower resistivities than the native materials they replace. Consequently, 3D effects should be of more concern in fractured, resistive rocks than in nonindurated sands, silts, clays and gravels.

Some researchers have identified borehole inversion effects in their cross-borehole ERT images. Daily and Ramirez (1995) conducted an ERT experiment to monitor *in situ* trichloroethylene (TCE) remediation by air sparging. Their tomograms revealed resistive sheaths around the boreholes. Bentonite drilling mud was interpreted to have seeped into the formation sands forming a conductive skin. Bentonite infiltration is a common occurrence and often forms a mud-cake on the walls of the borehole. On the basis of numerical modeling, the authors concluded that complex current flow conditions attributed to the presence of the bentonite mud caused the reconstruction algorithm to produce a resistive sheath artifact because the borehole conditions violated the 2D restriction in the finite element forward algorithm. Slater et al. (1997) used a 2.5D code to invert ERT data collected during a conductive tracer test in fractured limestone to delineate fractures. The downhole electrodes were located in fresh-water filled boreholes. Some of the results from Slater et al. (1997) have been rein-

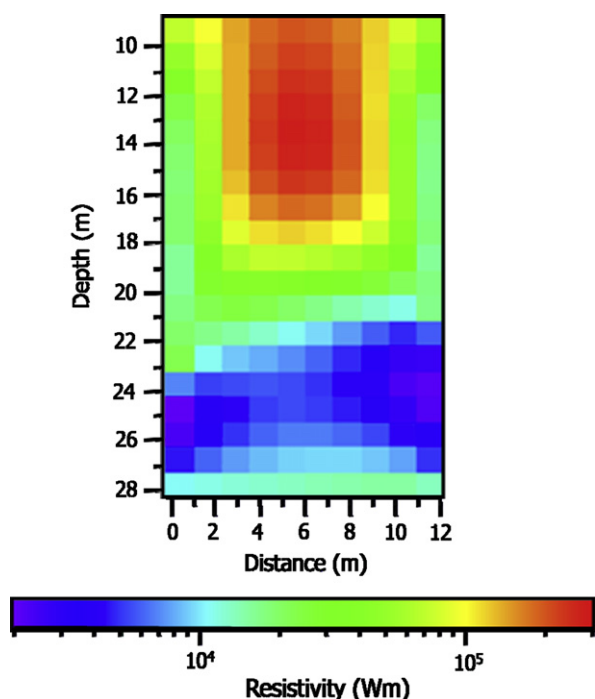


Figure 1 Resistivity image of borehole inversion effects (shown as relative resistivity high in red) modified from Slater et al. (1997).

terpreted by Daily et al. (2005) as artifacts resulting from borehole inversion effects. Fig. 1 presents an image of the 2.5D inversion results from Slater et al. (1997) where the heavily fractured zone at around 25-m depth can be seen as a low resistivity contrast to the background, but the large high resistivity ($>2 \times 10^5 \Omega\text{m}$) in the center of the image appears to be a result of the 2D resistivity model compensating for the low resistivity along the borehole.

Another type of 3D effect results from the use of a 2.5D code to invert ERT data for a target body with contrasting resistivity (e.g. solute plume), where the body is located outside the image plane. These shadow effects are artifacts generated by the 2D model as a numerical solution to data derived for an incomplete 3D problem (i.e. the effects of disturbance of the electric field within the image plane from a heterogeneity located outside of the image plane), combined with the reduced resolution of the model at the center volume compared to areas near the electrodes. Vanderborght et al. (2005) noted this effect as causing the deviation of breakthrough curves between simulated and inverted data; they showed that the inverted images had more of a diffuse character.

Purpose and overview of the experiments

The purpose of this paper is to evaluate the potential significance of ERT 3D effects on potential tomogram misinterpretations by examination of (1) borehole inversion effects, where the resistivity of the borehole fill contrasts with the host material and (2) shadow effects, where a 3D heterogeneity is located outside of the image plane. The results presented herein have important ramifications relative

to the application of ERT data to calibrate flow and transport models (e.g. Binley et al., 2002; Kemna et al., 2002; Vanderborght et al., 2005; Singha and Gorelick, 2005).

Synthetic data are created using a 3D forward model. The data are then inverted using a 2D code to generate a resistivity array along the image plane between two boreholes. Borehole inversion effects are evaluated by simulating two boreholes filled with material with contrasting resistivity relative to the host material. In addition, the significance of borehole diameter is demonstrated by incorporation of a buried, cubic-shaped, conductive heterogeneity ('target') between the boreholes to illustrate how borehole inversion effects influence target image resolution. Shadow effects are evaluated by comparing the results of simulations with the target centered and off-centered in the x -direction (left–right), and shifted out of the image plane in the y -direction. While the 3D effects evaluated in this paper are specific to the conditions modeled, the results should be applicable at the field scale.

Forward and inversion models

A 3D forward model is used to simulate a dipole–dipole ERT measurement array, and generate the transfer resistances (the voltage between an electrode pair divided by the current injected between another pair) based on the input resistivity values. The 3D forward model within the code R3 (Binley, 2007b) is used. The resistance values generated by R3 are used as input for a numerical, 2.5D inversion model R2 (Binley, 2007a) to generate a single 2D resistivity distribution that best represents the 'measured' data.

Forward model

Assuming a 3D distribution of isotropic conductivity, the forward model may be defined by the equation for point-source current I as:

$$\frac{\partial}{\partial x} \left(\frac{1}{\rho} \frac{\partial V}{\partial x} \right) + \frac{\partial}{\partial y} \left(\frac{1}{\rho} \frac{\partial V}{\partial y} \right) + \frac{\partial}{\partial z} \left(\frac{1}{\rho} \frac{\partial V}{\partial z} \right) = -I \delta(x) \delta(y) \delta(z), \quad (1)$$

subject to boundary conditions:

$$\frac{1}{\rho} \frac{\partial V}{\partial n} + \beta V = 0, \quad (2)$$

where V is the potential, δ is the Dirac delta function, n is the outward normal and β defines the boundary type. For the cases here Neumann boundary conditions ($\beta = 0$) are defined along all size faces of the boundary of the mesh.

R3's forward model is based on a finite element solution of Eq. (1) using linear hexahedral finite elements in an irregular mesh. The resistivity can vary from element to element but is uniform within each element. Electrodes are simulated as point locations, defined at nodes within the finite element mesh. The linear equations resulting from each finite element formulation are solved using a diagonally preconditioned conjugate gradient algorithm. The R3 code has been tested and utilized in a number of ERT studies to date (e.g. Binley et al., 2002; French and Binley, 2004; Singha and Gorelick, 2005; Looms et al., 2008).

Inversion model

The inverse model attempts to determine the distribution of resistivity that best matches the observed voltage potential data subject to specific constraints or penalty functions. The R2 code is based on the widely used Occam's approach of [deGroot Hedlin and Constable \(1990\)](#). The area under investigation is parameterized using a 2D finite element mesh: parameters are defined as cells of uniform resistivity, each cell being a finite element or group of adjacent finite elements. The resistivity distribution is solved by the model using a minimization of the objective function:

$$\Phi(m) = [D - F(m)]^T W^{-1} [D - F(m)] + \alpha m^T R m, \quad (3)$$

where $m = \log_e(\rho^{-1})$ in each parameter cell; D is the vector of measured transfer resistances; $F(m)$ contains the corresponding forward model resistances due to parameters m ; W is the vector of data variances used to weight individual measurements; R is the roughness matrix used to force smoothing of the resistivity distribution and to stabilize the inverse solution; α is a smoothing parameter.

In R2 the forward model $F(m)$ is computed on an irregular quadrilateral finite element mesh and accounts for current flow in 3D using the Fourier transformation defined in [Kemna \(2000\)](#). Eq. (3) is minimized in R2 using a Gauss Newton approach, which results in the iterative equations ([Binley and Kemna, 2005](#)):

$$(J_k^T W^{-1} J_k + \alpha R) \Delta m_k = J_k^T W^{-1} [D - F(m)] - \alpha R m$$

$$m_{k+1} = m_k + \Delta m_k, \quad k = 1, 2, 3, \dots \quad (4)$$

In Eq. (4) J is the Jacobian (or sensitivity) matrix evaluated for the current model. This matrix is computed using the principle of reciprocity, as described in detail by [Kemna \(2000\)](#).

In order to obtain a stable solution of Eq. (4) regularization through the combination of the smoothing parameter α and roughness matrix R is essential. In R2, the 'roughness' matrix, R , in Eq. (3) is based on a three-point (in each direction) quadratic filter. The smoothing parameter α is optimized at each iteration, k , of the inversion using a line search (as in, e.g. [deGroot Hedlin and Constable, 1990](#)). As the iterative procedure progresses, the value of α decreases as data misfit becomes more dominant towards the end of the iterative search.

Modeling artifacts

Borehole inversion effects

The voltage near a buried, single point-source of current in an infinite, homogeneous medium is represented by ([Telford et al., 1990](#)):

$$V = \left(\frac{I\rho}{4\pi} \right) \frac{1}{r} \quad (5)$$

where V is the voltage, ρ is the resistivity, r is the distance from the current electrode and I is the current. Current flow near a single, point-source of current embedded in a borehole filled with a conductive material is dependent on the shape and depth of the borehole, and the conductivity contrast between the fill material and the geologic material

forming the borehole walls ([Osiensky et al., 2004](#)). Current flow near the electrode generally is not spherical as indicated in Eq. (5). No direct analytical solutions exist for this problem. Therefore, the analysis of borehole effects is performed through numerical modeling.

Two hypothetical borehole conditions were simulated numerically to illustrate equipotentials about a point-source of current. Fig. 2 presents two example cross-sectional-contour maps of voltages near a current electrode buried 1.5 m below ground level for a current of 0.5 A. Case 1 shows the voltages about the current electrode in a homogeneous formation without the presence of a borehole. Case 2 is more realistic with the current electrode placed in a borehole with fill of contrasting resistivity relative to the formation. The 0.15-m diameter borehole has a fill resistivity of $1 \mu\Omega$. The resistivity of the formation is $100 \mu\Omega$. These values, e.g. may represent a clay-filled borehole within a sandstone unit. The contour maps illustrate differences in current flow due to the presence of the partially penetrating borehole with two orders of magnitude contrast in resistivity. A point-source of current in a conductive, partially penetrating cylinder causes preferential flow in the borehole whereby the current density is decreased (i.e. decrease in current per unit area of cross section). In effect, the filled borehole approximates a cylindrical electrode compared to a true point-source. Fig. 2c is a contour map of voltage ratios (case 2/case 1) to depict spatial changes in the voltage distribution between the two cases. Based on Eq. (3), the addition of a low resistivity fill material results in a lower voltage at a given distance than would be predicted for the native material alone. Thus, ratio values greater than 1.0 depict areas that appear to be more resistive; ratio values less than 1.0 depict areas that appear to be more conductive. It is obvious that the existence of the filled borehole for case 2 changed the distribution of voltages about the current electrode compared to case 1 without a borehole. Unless information about the borehole characteristics and borehole fill are provided as input data, the inversion model incorrectly interprets spatial changes in voltages outside of the borehole as a spatial change in apparent resistivity. Thus, borehole inversion effects result as the forward solver attempts to resolve the discrepancy in the voltages for numerous electrode pairs into meaningful changes in resistivity.

Shadow effects

During the forward model simulations of a buried conductive heterogeneity without the presence of boreholes, the electric field is refracted relative to the homogeneous case. When the target is located outside of the 2D image plane (e.g. as during cross-hole ERT between two boreholes), the resultant refractions in the electric field are misinterpreted by 2.5D inversion algorithms as a body within the image plane. The inversion attempts to resolve the cause of the refraction without adequate information. The algorithm generates reasonable resistances for the refracted electric field to produce a resistivity array that includes shadows of the heterogeneity. [Shima \(1989, 1992\)](#) suggests that the effect of anomalies lying outside the interest area can be reduced, and the uniqueness of the inversions can be improved by using a combination of measurements from along boreholes and cross-borehole. [Shima \(1989\)](#) also suggests

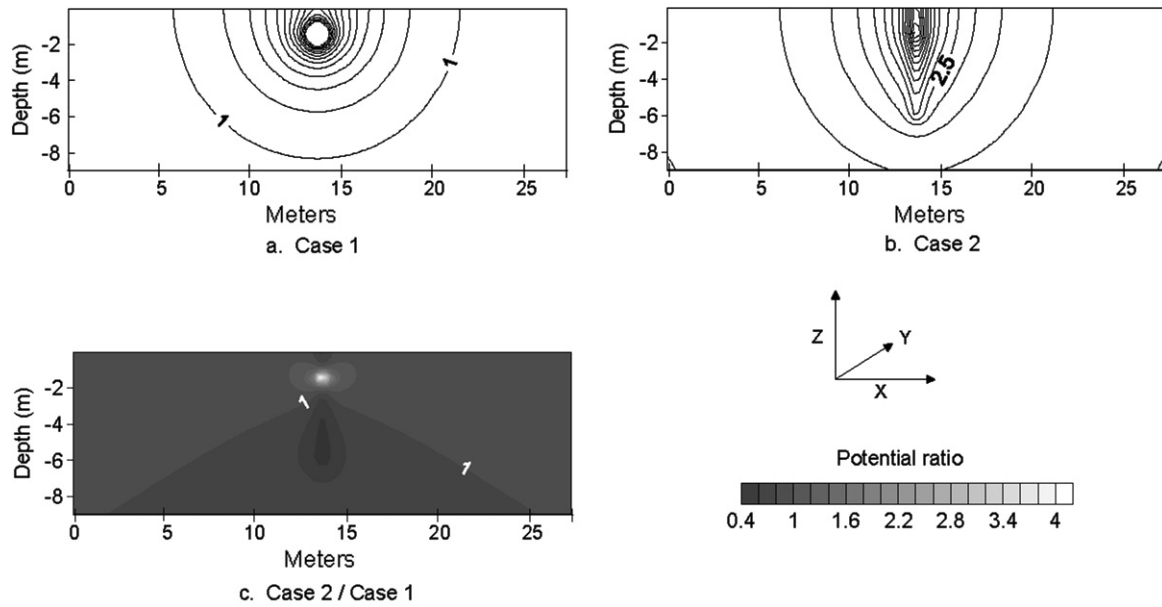


Figure 2 (a) Case 1 – voltages (mV) for a buried current electrode without a borehole (100 μm homogeneous half space). The current electrode is located at a depth of 1.5 m. (b) Case 2 – voltages for a buried current electrode in a conductive borehole with a resistivity of 1 μm ; boreholes are 6 m long. (c) Ratio of case 2/case 1 depicting the spatial changes in apparent resistivity due to the presence of the borehole. Contour interval for (a and b) is 1 mV, and (c) is 0.2.

examining a larger area to include outside the objective area for a more enhanced interpretation within the objective region. Sasaki (1992) recommends choosing a block discretization consistent with the resistivity ranges inside and outside the target region.

When a heterogeneity with a contrasting resistivity lies outside, but near, the image plane, the effects of the electrical field refraction propagates through the image plane resulting in false changes in apparent resistivity. Fig. 3 presents a cross-sectional contour map of voltage ratios near a current electrode showing changes from a homogeneous resistivity distribution caused by a hypothetical target het-

erogeneity located completely out of the image plane ($y = 0$) (target case/uniform case). The outer edge of the target (2 m \times 2 m \times 2 m) is located 3 m in front of the image plane; the geometric center is located at a depth of 1.5 m. The resistivity of the target is 1 μm , and the uniform background resistivity is 100 μm . The presence of the target caused refraction of the electric field. Both resistive and conductive changes are detected in the image plane with poor resolution of the actual target. Fig. 3 shows an example for one current electrode location. Errors exist for all the electrode pair combinations. Although the errors may small, they constitute another source of additive errors.

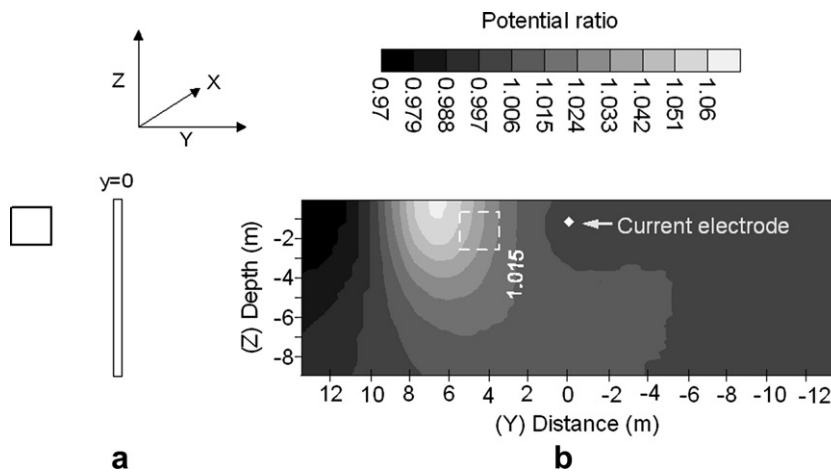


Figure 3 (a) Orthogonal view of a target heterogeneity, side located 3 m in front of the image plane ($y = 0$), (b) ratio of voltages (target case/uniform case) for (a) ($x = 0$) depicting the spatial changes in voltage caused by the addition of the target (represented by dashed box). Current = 0.5 A.

Cross-borehole synthetic data models

In our synthetic ERT experiments, two boreholes are fitted with several electrodes to image the resistivity distribution in the volume between the boreholes. Forward and inverse model grids are used to simulate field experiments containing possible borehole inversion effects and shadow effects. Several simulations are performed to evaluate various borehole conditions, and positions of a single heterogeneity, on the inversion results.

Forward solution

A model was defined to simulate ERT data collected in two 15-m long vertical boreholes, 10 m apart, each containing 16 equally spaced electrodes. The 3D forward model utilizes a $61 \times 45 \times 47$ hexahedral mesh covering a region $260 \text{ m} \times 254 \text{ m} \times 140 \text{ m}$ to account for current flow towards infinite boundaries. Within the 3D mesh, element sizes in the x- and y-directions increase away from the centrally located boreholes. In the (vertical) z-direction, element sizes increase with depth below the bottom of the boreholes. Accuracy of the solution was tested by comparing numerical model results with those from a uniform half space, for which an analytical solution can be derived. The grid was considered appropriate when all simulated measurements showed errors less than 2%.

Cross-borehole ERT experiments are conducted in boreholes, typically with a 0.1 m or greater diameter attributed to common drilling limitations, and to allow for multiple uses (e.g. monitoring, sampling and injection). Because of the hexahedral finite elements used in the 3D model, the two boreholes for the modeled ERT experiments are simulated as prismatic heterogeneities, and not as actual cylinders. Therefore, the results of the study are not geometrically exact. Although not tested, it is anticipated the differences are minor. Boreholes with 0.1 m diameters are simulated except where noted. Prisms composed of $2 \times 2 \times 30$ cubic elements are used to simulate the 15-m long boreholes. Fig. 4 shows a cross-sectional view of a small portion of the forward model mesh in the borehole area. Prisms composed of $4 \times 4 \times 30$ elements are used to simulate 0.2 m-diameter boreholes for comparison.

A 'skip-2' measurement schedule is applied in which two electrodes separate the current electrode pair (or potential electrode pair), i.e. a dipole length of 3 m is used. This measurement schedule is used to increase the resolution further away from the borehole compared to an electrode pair with a smaller separation distance, while maintaining good resolution near the boreholes. In addition, this skip schedule improves the signal to noise ratio (Slater et al., 2000). Evaluation of different electrode configurations is described by Zhou and Greenhalgh (2000).

A baseline forward model was developed with a uniform resistivity of $100 \mu\text{m}$. Two percent random (Gaussian) noise was added to approximate conditions typical of field data.

Numerical inversion

The inverse problem uses a different mesh than the forward model, which is common practice (Binley et al., 1996). The

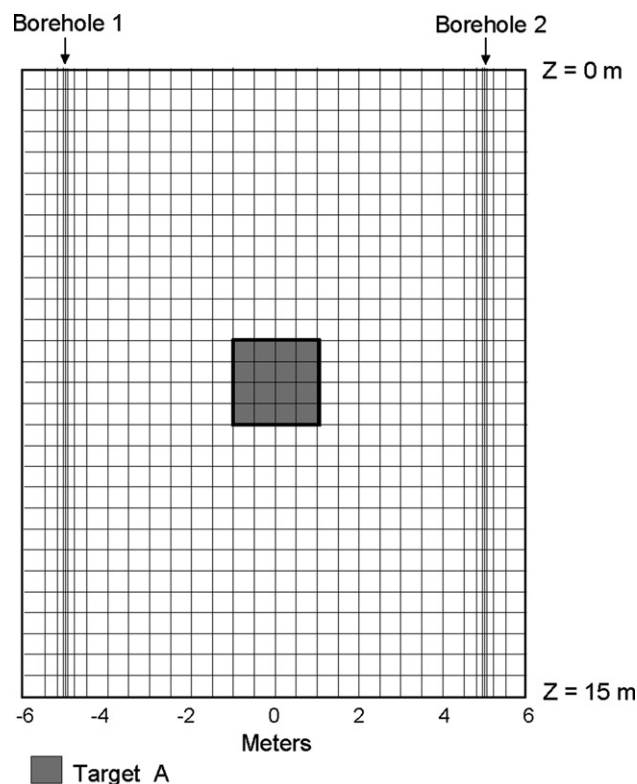


Figure 4 Cross-sectional view of a small portion of the 3D forward model mesh showing the grid spacings near the two boreholes. The location of a single, 8 m^3 cubic heterogeneity (target A) is shown between the boreholes. Boreholes are located 10 m apart. One electrode is located in each 1 m thick layer in each borehole.

inversion model uses a node-centered, 2D, quadrilateral mesh composed of 52×46 square elements (Fig. 5) and was chosen based on previous ERT experiments. Outside the area shown in Fig. 5 the elements increase in size away from the boreholes. The mesh is parameterized into resistivity blocks of four (2×2) elements. Each borehole location is defined by a column of 16 electrodes on 1-m spacings. The data weight matrix, W , in Eq. (3) was set to be consistent with the applied random noise.

Model simulations and results analysis

Selected conditions were simulated to evaluate potential 3D borehole inversion effects and shadow effects in ERT experiments. Borehole inversion effects were examined by modeling several sets of conditions, each simulating ERT between two boreholes. The first set of conditions has a one order of magnitude contrast between the borehole-fill material and the host formation. The next model simulates a borehole-fill material with two orders of magnitude contrast with the host formation. The borehole diameter is doubled to evaluate the potential significance of hole size on borehole inversion effects. A cubic heterogeneity (target A) is introduced between the boreholes (see Fig. 4 for location) to evaluate the significance of borehole inversion effects on the ERT image precision.

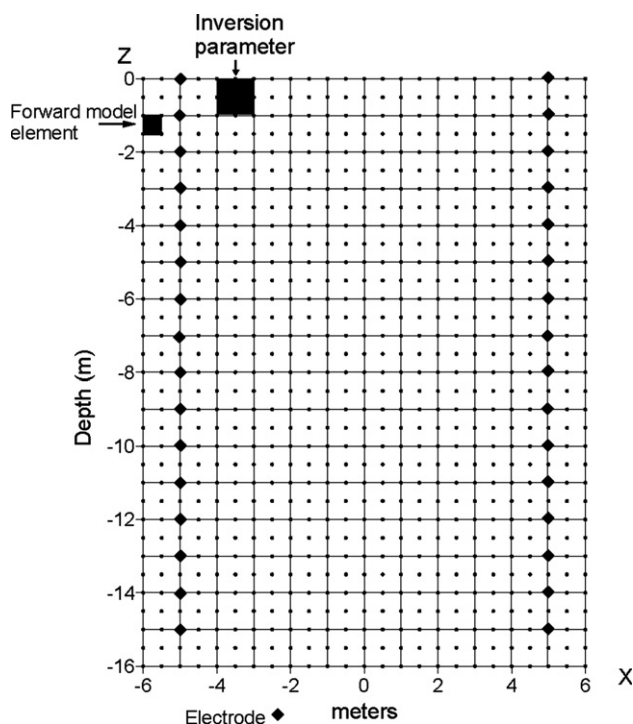


Figure 5 A small portion of the finite element inversion model mesh and inversion parameterization in the borehole areas for the inversion process. Mesh extends beyond what is shown to reduce the effects of boundary conditions. Scales are in meters.

To study shadow effects, target A, centered in the y -direction ($y = 0$) in previous simulations, is repositioned at distances of 1, 3 and 5 m (i.e. $y = 1$ m, $y = 3$ m and $y = 5$ m) away from the image plane in separate simulations. In the x -direction, target A was centered ($x = 4$ to 6 m) and off-centered ($x = 2$ to 4 m) in separate simulations. The background resistivity for all simulations was $100 \mu\text{m}$ (\log_{10} -resistivity = $2 \mu\text{m}$). All tomograms are presented on \log_{10} -resistivity scales for visual clarity. Not all the resultant tomograms of the model simulations presented share a common resistivity scale because the purpose of this work is to illustrate characteristic artifacts and subtle differences that otherwise might be masked.

The resolution of ERT is a function of many factors including data accuracy, electrode geometry, electrode sampling schemes, and other factors (Daily and Ramirez, 1995). Changes in the measurement scheme, number of electrodes, and the variables in the model itself (e.g. smoothing factors) lead to different solutions. Four grid elements compose the smallest area that can be resolved by the inversion model developed for this investigation because a single parameter is 2×2 . Although the model simulations represent simplified conditions, general characteristics of borehole inversion effects, and shadow effects are illustrated relative to tomograms typical of cross-borehole ERT field experiments.

Borehole effects

Two simulations of ERT between two 0.1-m diameter boreholes were conducted with contrasting borehole fill from

the host formation to illustrate borehole effects a function of the fill contrast. One simulation with a borehole fill resistivity of $10 \mu\text{m}$ (\log_{10} -resistivity = $1 \mu\text{m}$) and the second simulation with a borehole fill resistivity of $1 \mu\text{m}$ (\log_{10} -resistivity = $0 \mu\text{m}$). Fig. 6a shows the image of a borehole fill/formation resistivity contrast $BH\rho_{\text{Contrast}} = 0.10$. There is very little change from the uniform case. Fig. 6b is an image with a value of $BH\rho_{\text{Contrast}} = 0.01$. Artifacts resulting from borehole inversion effects are evident as the highly resistive borders that frame the image, particularly the columns that parallel the boreholes and the conductive zone that is imaged between the boreholes. These artifacts result from preferential current flow up and down the borehole rather than directly into the formation, causing the inversion algorithm to generate artifacts to account for the apparent decrease in current density within the borehole relative to the absence of borehole fill, and distortions in the electric field.

Two 0.2 m-diameter boreholes with contrasting fill resistivities were simulated to illustrate the significance of borehole diameter on borehole inversion effects. Each borehole was represented (in plan) as four elements wide in the x - and z -directions. This required a slight modification to the model grid used to simulate 0.1-m diameter boreholes.

The first model used $BH\rho_{\text{Contrast}} = 0.1$ and the second model used $BH\rho_{\text{Contrast}} = 0.01$. Fig. 6c shows the results for $BH\rho_{\text{Contrast}} = 0.1$. Fig. 6d shows the results for $BH\rho_{\text{Contrast}} = 0.01$. Comparison of Fig. 6a with Fig. 6c and b with Fig. 6d demonstrates that increasing the borehole diameter causes the resistive artifacts to intensify. The resistivity patterns between Fig. 6c and d are similar because the geometry of current flow is similar for both scenarios. Inaccuracies created by the 2D forward solver during the inversion process are greater for the larger diameter boreholes, resulting in greater borehole effects.

Borehole inversion effects plus heterogeneity

A $2 \text{ m} \times 2 \text{ m} \times 2 \text{ m}$ cubic heterogeneity is modeled initially in a homogeneous medium without boreholes, and then again with boreholes of contrasting resistivities in order to evaluate interferences by borehole inversion effects. Fig. 7 shows the locations of the four named targets. Target A_c is centered in the x -direction; target A_{nc} is non-centered in the x -direction. The resistivity contrast of the target (the ratio of the target resistivity/formation resistivity) was $T\rho_{\text{Contrast}} = 0.01$ for these model simulations. The target resistivity was $1 \mu\text{m}$ (\log_{10} resistivity = $0 \mu\text{m}$) within a formation of resistivity $100 \mu\text{m}$ (\log_{10} resistivity = $2 \mu\text{m}$).

Centered target (target A_c)

Fig. 8a is a tomogram showing the resolution of target A_c with $T\rho_{\text{Contrast}} = 0.01$ within a uniform formation without boreholes (i.e. $BH\rho_{\text{Contrast}} = 1.0$). Target A_c is imaged as a resistivity low. However, an increase in resistivity is seen outside the target area due to the regularization of the inversion. The large size of the anomaly relative to the actual target body, and the weakness of the recovered contrast in resistivity relative to the background is indicative of the weak sensitivity of ERT away from the electrodes coupled with the limited extent of the target (2 m) normal to the image plane.

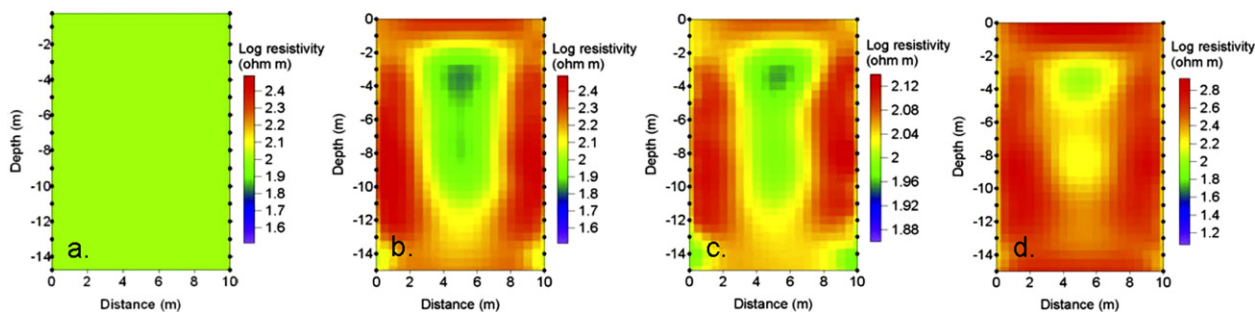


Figure 6 Tomograms of borehole with different resistivity contrasts and different borehole diameters. (a) and (b) have 0.1-m diameter boreholes; (c) and (d) have 0.2-m diameter boreholes. (a) and (c) have a $BH\rho_{\text{Contrast}} = 0.10$. (b) and (d) have a $BH\rho_{\text{Contrast}} = 0.01$ (note that the log resistivity scales differ for the larger-sized boreholes). Electrode locations are shown as solid circles. No target heterogeneity exists between the boreholes for these simulations.

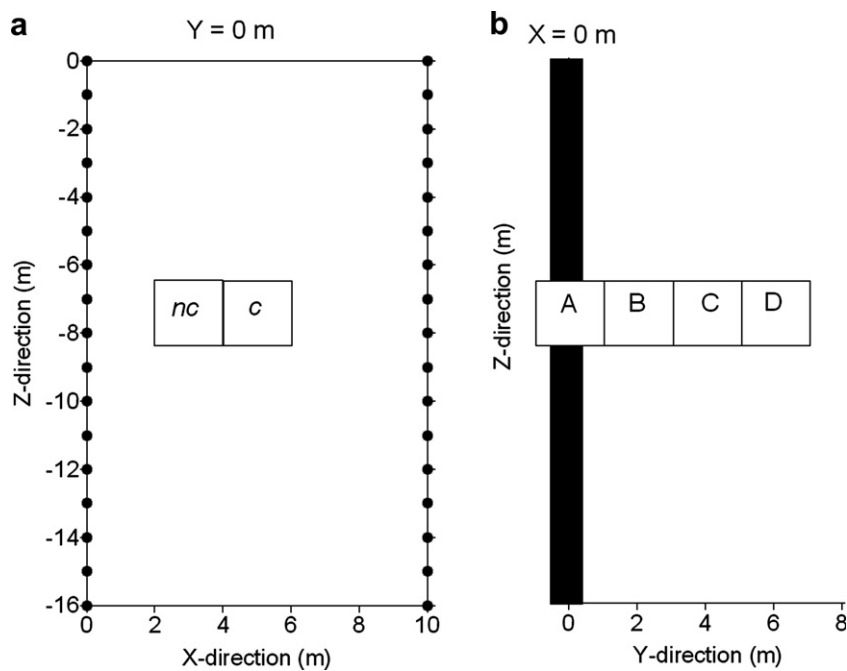


Figure 7 Diagram showing 8 m^3 target locations (circles represent electrodes). (a) $y = 0 \text{ m}$ plane, subscript nc represents a target that is not centered and subscript c represents a target that is centered. (b) $x = 0$ plane; targets B, C and D are used in shadow effect simulations.

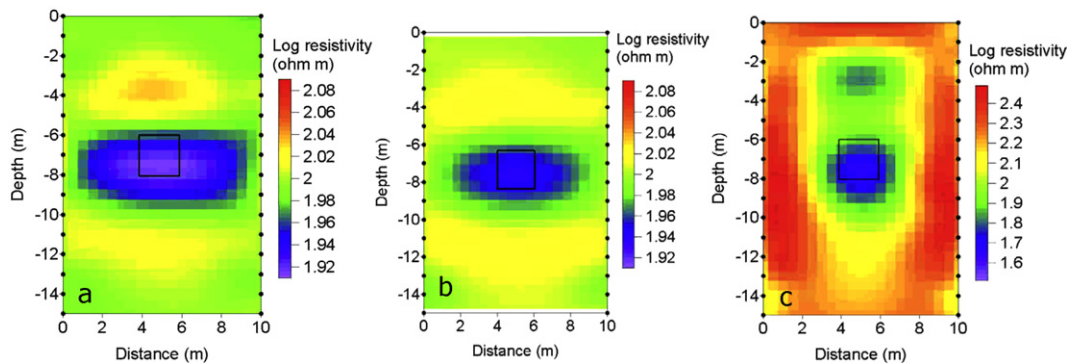


Figure 8 Tomograms of a centered 8 m^3 cube (represented by box), target A_c , with $T\rho_{\text{Contrast}} = 0.01$: (a) no boreholes, (b) two boreholes with $BH\rho_{\text{Contrast}} = 0.1$ and (c) two boreholes with $BH\rho_{\text{Contrast}} = 0.01$.

Two additional model runs were completed to simulate target A_c between two conductive boreholes. Fig. 8b shows the resultant image for $BH\rho_{\text{Contrast}} = 0.10$ and $T\rho_{\text{Contrast}} = 0.01$. Target A_c is detected at the correct location as a resistivity low. However, by increasing the contrast of the borehole resistivity $BH\rho_{\text{Contrast}} = 0.01$ by one order of magnitude (smaller ratio value), the perimeter of the image in Fig. 8c reveals significant borehole effects. A conductive artifact also materializes above the target. Despite these artifacts, there is a better definition of the inverted target resistivity. Table 1 lists the arithmetic-mean resistivity values (of four center-most elements) derived by the inversion model at the location of the geometric center of Target A_c for various modeled scenarios. Based on the images in Fig. 8 and/or data from Table 1, the following observations are noteworthy: (1) $BH\rho_{\text{Contrast}} = 0.01$ causes the inverted resistivity at the geometric center of target A_c , and the target size to be reproduced more accurately than without borehole inversion effects and (2) $BH\rho_{\text{Contrast}} = 0.10$ improves the resolution of target A_c inverted resistivity, and target location is reproduced accurately; however, target size is overestimated significantly for the reasons described above.

Non-centered target (target A_{nc})

To evaluate resolution for targets not exactly centered between two columns of electrodes, target A_{nc} with $T\rho_{\text{Contrast}} = 0.01$ is offset 2 m (see Fig. 7a for location). Fig. 9a shows the inverted resistivity distribution for target A_{nc} in an otherwise uniform formation without the presence of boreholes. The imaged resistivity low more accurately represents the true target resistivity compared to that for the centered target. This is attributed to a better sensitivity near the electrodes, yet the lowest resistivity is shifted 1.25 m to the left of the target's geometric center. Fig. 9b shows the inversion model results for the target between two boreholes with $BH\rho_{\text{Contrast}} = 0.01$. Target dimensions are better approximated by the imaged anomaly compared to the results for target A_{nc} without the presence of boreholes. Borehole inversion effects cause the resistivity low to be shifted 1.75 m to the right in the x-direction from the position of target A_{nc} by overwhelming the influence of the target. These simulations demonstrate borehole inversion effects could have positive ramifications relative to target definition if some information about the target is known *a*

priori; however, misinterpretations relative to interpretation of target details are also possible.

Reduction of borehole inversion effects for time-lapse studies

Reduction of borehole inversion effects is crucial for ERT experiments when the shape and character of the target are not known *a priori*. Where the collection of time sequenced data is possible, analysis of ERT field data as inverted ratios of R_{rat} reduces the borehole inversion effects if the resistivity of the borehole fill/fluid remains relatively unchanged between data collection periods. R_{rat} is defined as (Daily et al., 1995):

$$R_{\text{rat}} = \left(\frac{R_{t2}}{R_{t1}} \right) * R_h \quad (5)$$

where R_{t1} transfer resistance at time t_1 , R_{t2} is the transfer resistance at a subsequent time t_2 , and R_h is the transfer resistance for the homogeneous resistivity distribution predicted by the forward model synthetic test case.

Fig. 10 is an image of the inverted R_{rat} values, where the baseline case has two boreholes with $BH\rho_{\text{Contrast}} = 0.01$, and the subsequent case also incorporates target A_c (centered target) with $T\rho_{\text{Contrast}} = 0.01$. These were simulated to evaluate the condition of a target developing between measurement periods (e.g. during a tracer test). Though showing a cleaner picture by reducing borehole effects significantly, Fig. 10 shows that the details of target A_c are lost in comparison with Fig. 8c, the case of borehole inversion effects included. These results suggest that borehole inversion effects may actually be advantageous when the data are imaged both ways (single data sets plus ratio data sets) depending on the size, shape, orientation and location of the target. Borehole inversion effects enhance the contrast of the target (Table 1), and result in an image that more accurately represents its size in this case. In fact, the geometric mean resistivity distribution at target A_c derived by inversion of R_{rat} values is actually 10% greater than the resistivity for the case of target A_c without boreholes, whereby definition of the target is diminished. Inversion of R_{rat} values provides a means to differentiate anomalies from artifacts. One can qualitatively determine the degree of the borehole inversion effects by comparison of the data imaged both ways.

Table 1 The arithmetic-mean resistivity values (of four center-most elements) derived by the inversion model at the location of the geometric center of the targets for various modeled scenarios

| | Target name | Arithmetic-mean resistivity (Ωm) at geometric center of target within $y = 0$ plane | |
|-----------------------------------|-------------|---|--------------|
| | | Centered | Non-centered |
| No BH | None | 81.87 | 74.41 |
| $BH\rho_{\text{Contrast}} = 0.10$ | Target A | 87.08 | 77.09 |
| $BH\rho_{\text{Contrast}} = 0.01$ | Target A | 46.92 | 65.85 |
| BH ratio | Target A | 90.06 | NA |
| Shadow: out 1 m | Target B | 89.17 | 87.61 |
| Shadow: out 3 m | Target C | 97.38 | 99.97 |

Resistivity of targets B and C is 1 Ωm . Resistivity of the background is 100 Ωm . NA, not applicable.

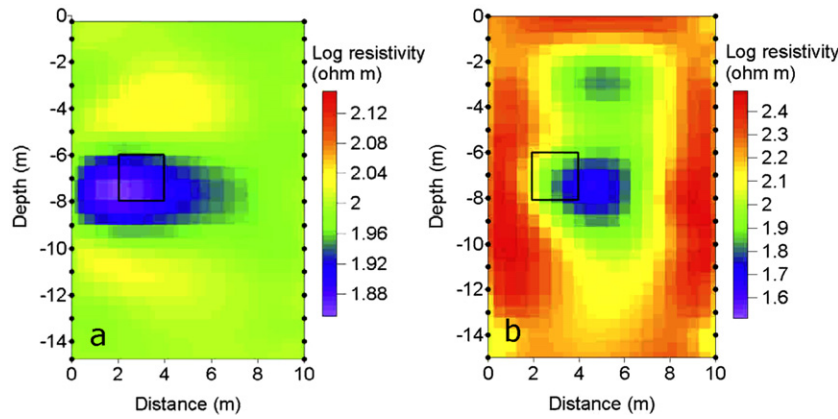


Figure 9 Images of a non-centered, 8 m^3 cube (represented by box) (target A_{nc}): (a) two columns of electrodes without boreholes and (b) columns of electrodes in two boreholes with $BH\rho_{\text{Contrast}} = 0.01$.

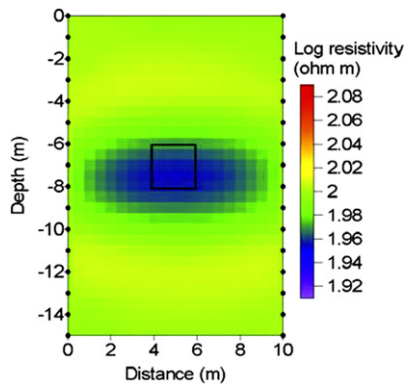


Figure 10 Image of inverted R_{rat} values, where R_{t1} has two boreholes with a $BH\rho_{\text{Contrast}} = 0.01$, and R_{t2} also incorporates target A_c with a $T\rho_{\text{Contrast}} = 0.01$.

Shadow effects

Inversion artifacts may also result from the use of 2D inversion codes for 3D structures located outside the 2D image plane. Development of inversion shadow effects is evaluated for an 8 m^3 , target heterogeneity with $T\rho_{\text{Contrast}} = 0.01$ where the edge is located out of the image plane ($y = 0 \text{ m}$) by distances of $y = 1 \text{ m}$ (target B), $y = 3 \text{ m}$ (target C) and $y = 5 \text{ m}$ (target D) (see Fig. 7 for locations).

Modeled results for target B are shown as images in Fig. 11. Fig. 11a shows the image for target B_c (centered in the x -direction between two columns of electrodes), and Fig. 11b shows the image for target B_{nc} (2 m to the left of center) between the same two columns of electrodes. In both instances the resistivity low is a shadow of the target and is actually an artifact rather than the true anomaly. The 2D inversion code interprets the refracted electric field as a change in the resistivity distribution causing a shadow of the target to be generated within the image plane. Therefore, what appears to be an accurately located target actually is located 1 m away in the y -direction.

Table 1 lists calculated arithmetic-mean resistivity values within the image plane ($y = 0$) at the center of targets B and C in the x - and z -directions; there is no change from the homogeneous distribution with the inclusion of target

D. In comparison to the data for target A, the shadow resistivities for targets B and C are greater (i.e. the effects weaken, as expected, as the target is moved away from the image plane). The centered and non-centered targets show some minor contrast in shadow effects for the cases considered. Target C results in less than 5% change from homogeneous conditions with the absence of the target (Fig. 12). Target C_{nc} causes essentially no change from the homogeneous resistivity distribution. Fig. 12 illustrates that the model response to target B is affected more when the target is located nearer to the electrodes and less than 1.5 m from the image plane. However, the shadow of target C_c is detectable at a distance of 3 m from the image plane unlike the target C_{nc} . These results demonstrate the impact of the 3D sensitivity of ERT data, which is also likely to be dependent on the measurement scheme adopted: larger dipole lengths are likely to lead to greater sensitivity to off-plane subsurface heterogeneity.

Conclusions

Conventional 2.5D inversion algorithms misinterpret the voltage distribution from a 3D body causing errors in the resultant resistivity distribution. The modeling results reported here show that borehole effects are proportional to the contrast in borehole resistivity relative to the formation resistivity. 2.5D inversion algorithms may misrepresent the location of a target heterogeneity located between two boreholes or completely mask it altogether due to borehole effects. A significant potential ramification of artifacts being confused for anomalies may be the incorrect placement of monitoring, extraction, or treatment wells. For example, an apparently conductive zone could lead to well sitings intended to take advantage of a possible preferential pathway that may in fact not exist. However, analysis of time-sequenced data sets, e.g. using ratioed resistance data, may help to reduce borehole inversion effects, and thus the risk of misinterpretations.

The presence of a heterogeneity located outside the image plane can influence cross-borehole ERT data. Our results demonstrate that shadow effects are dependent upon the target location within the plane and distance from

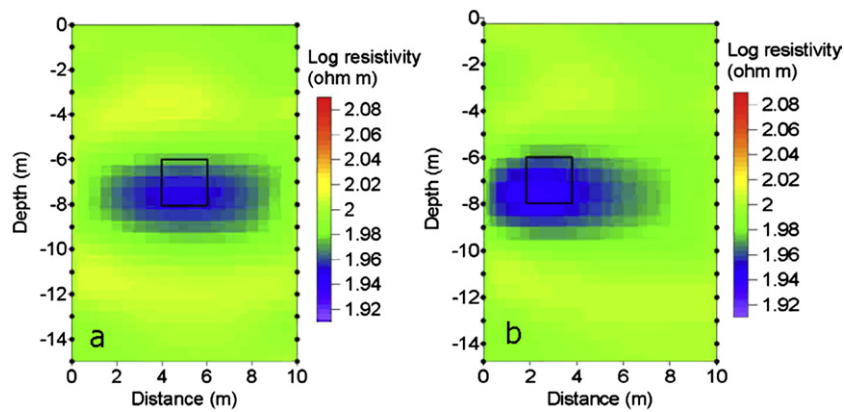


Figure 11 Image of shadow effects (resistivity low) caused by target B (8 m^3 cube represented by box) with $T_{\rho\text{Contrast}} = 0.01$ out of y-plane by 1 m: (a) target B_c and (b) target B_{nc} .

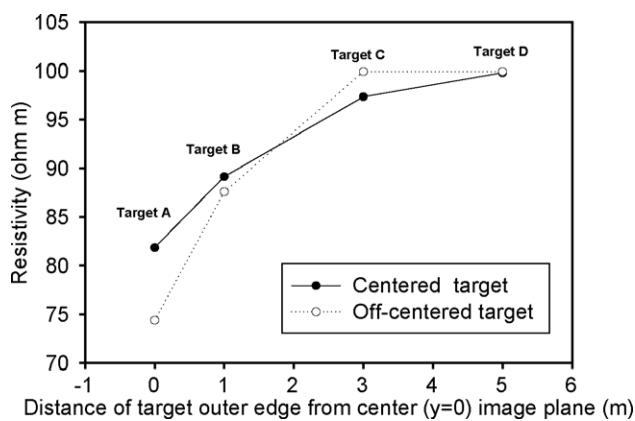


Figure 12 Graph of arithmetic mean resistivity within the image plane at the center of the target in the x- and z-directions for centered ($x = 4\text{--}6 \text{ m}$) and non-centered ($x = 2\text{--}4 \text{ m}$) targets. Actual target resistivities are $1 \mu\text{m}$.

the plane. Although not tested in this study, the distance to which shadow effects are inconsequential will be site-specific, and depend also on the size of the heterogeneity and its resistivity contrast to the host rock. The algorithm incorrectly represents the true homogeneous resistivity of the image plane through shadow effects and may result in misleading interpretations. This is a potentially a significant problem in site characterization and remediation design as described above for the borehole inversion effects. These results are also significant for analysis of tracer data using ERT: off-plane tracer mass may be incorrectly interpreted to be in-plane. Failure to account for such effects may result in inaccurate estimates of transport parameters, e.g. advection and dispersion.

3D effects in 2D electrical imaging will likely lead to false impressions about the size, shape and location of the target heterogeneity. Many downhole electrical geophysical experiments are conducted in boreholes with contrasting resistivity to the formation, and where the objective of the investigations is to locate or track a migrating contaminant plume between two boreholes. It will therefore be necessary for investigators to resolve the 3D impact by well

designed experiments. The following steps could be considered as helping to reduce borehole effects in the inversion:

1. minimize borehole diameter;
2. minimize the contrast between borehole fill materials and the native formation materials;
3. measure the resistivity of the borehole fill/water and use this within a 3D forward model as part of the inversion approach;
4. model changes in resistivity, e.g. using data ratios, for time-lapse studies.

Shadow effects can be reduced by reducing the dipole length of four electrode measurements; however, this may be detrimental to data quality and resolution within the image plane. One should, however, attempt to quantify the off-plane sensitivity in all cases where shadow effects may occur.

References

- Bear, J., Tsang, C-F., de Marsily, G., 1993. Flow and Contaminant Transport in Fractured Rock. Academic Press, San Diego, CA.
- Binley, A., 2007a. R2: Summary. Lancaster University, Lancaster, UK. Available from: <www.es.lancs.ac.uk/people/amb/Free-ware/R2/R2_summary.htm> (verified 27.04.08).
- Binley, A., 2007b. R3: Summary. Lancaster University, Lancaster, UK. Available from: <www.es.lancs.ac.uk/people/amb/Free-ware/R3/R3_summary.htm> (verified 27.04.08).
- Binley, A., Kemna, A., 2005. Electrical methods. In: Rubin, Y., Hubbard, S.S. (Eds.), Hydrogeophysics. Springer, pp. 129–156.
- Binley, A., Cassiani, G., Middleton, R., Winship, P., 2002. Vadose zone flow model parameterisation using cross-borehole radar and resistivity imaging. *J. Hydrol.* 267, 147–159.
- Binley, A.M., Shaw, B., Henry-Poulter, S., 1996. Flow pathways in porous media: electrical resistance tomography and dye straining image verification. *Measurement Sci. Technol.* 7 (3), 384–390.
- Daily, W., Ramirez, A., Binley, A., LaBrecque, D., 2005. Electrical resistance tomography – theory and practice. In: Butler, D.K. (Ed.), Near Surface Geophysics, Investigations in Geophysics No. 13. Society of Exploration Geophysicists, pp. 525–550.
- Daily, W., Ramirez, A., 1995. Electrical resistance tomography during in-situ trichloroethylene remediation at the Savannah River Site. *J. Appl. Geophys.* 33, 239–249.

- Daily, W., Ramirez, A., LaBrecque, D., Barber, W., 1995. Electrical resistance tomography experiments at the Oregon Graduate Institute. *J. Appl. Geophys.* 33, 227–237.
- Day-Lewis, F., Singha, K., Binley, A., 2005. On the limitations of applying petrophysical models to tomograms: a comparison of correlation loss for cross-hole electrical-resistivity and radar tomography. *J. Geophys. Res.* 110 (B8), B08206. doi:10.1029/2004JB00356.
- deGroot Hedlin, C., Constable, S., 1990. Occam's inversion to generate smooth, two-dimensional models from magnetotelluric data. *Geophysics* 55 (12), 1613–1624.
- French, H., Binley, A., 2004. Snowmelt infiltration: monitoring temporal and spatial variability using time-lapse geophysics. *J. Hydrol.* 297, 174–186.
- Keller, G.V., Frischknecht, F.C., 1966. *Electrical Methods in Geophysical Prospecting*. Pergamon Press, New York.
- Kemna, A., 2000. *Tomographic Inversion of Complex Resistivity-Theory and Application*, PhD Thesis. Bochum Ruhr-University, Germany (published by: Der Andere Verlag, Osnabrück, Germany).
- Kemna, A., Vanderborght, J., Kulesa, B., Vereecken, H., 2002. Imaging and characterisation of subsurface solute transport using electrical resistivity tomography (ERT) and equivalent transport models. *J. Hydrol.* 267, 125–146.
- LaBrecque, D.J., Ramirez, A.L., Daily, W.D., Binley, A.M., Schima, S.A., 1996. ERT monitoring of environmental remediation processes. *Measurement Sci. Technol.* 7 (3), 375–383.
- Looms, M.C., Binley, A., Jensen, K.H., Nielsen, L., Hansen, T.M., 2008. Identifying unsaturated hydraulic parameters using an integrated data fusion approach on cross-borehole geophysical data. *Vadose Zone J.* 7, 238–248.
- Osiensky, J.L., Nimmer, R.E., Binley, A.M., 2004. Borehole cylindrical noise during hole–surface and hole–hole resistivity measurements. *J. Hydrol.* 289 (1–4), 78–94.
- Parkhomenko, E.I., 1967. *Electrical Properties of Rocks*. Plenum Press, New York.
- Sasaki, Y., 1992. Resolution of resistivity tomography inferred from numerical simulation. *Geophys. Pros.* 40, 453–463.
- Shima, H., 1989. *Effects on Reconstructed Images of Surrounding Resistivity Structures in Resistivity Tomography*, Expanded Abstracts with Biographies. Technical Program, International SEG Meeting, vol. 59, pp. 385–389.
- Shima, H., 1992. 2-D and 3-D resistivity image reconstruction using crosshole data. *Geophysics* 57 (10), 1270–1281.
- Singha, K., Gorelick, S.M., 2005. Saline tracer visualized with three-dimensional electrical resistivity tomography: field scale spatial moment analysis. *Water Resour. Res.* 41, W05023.
- Slater, L.D., Binley, A., Brown, D., 1997. Electrical imaging of fractures using ground-water salinity change. *Ground Water* 35 (3), 436–442.
- Slater, L., Binley, A.M., Daily, W., Johnson, R., 2000. Cross-hole electrical imaging of a controlled saline tracer injection. *J. Appl. Geophys.* 44, 85–102.
- Telford, W.M., Geldart, L.P., Sheriff, R.E., 1990. *Prospecting Geophysical Methods*. Cambridge University Press, Cambridge.
- Vanderborght, J., Kemna, A., Hardelauf, H., Vereecken, H., 2005. Potential of electrical resistivity tomography to infer aquifer transport characteristics from tracer studies: a synthetic case study. *Water Resour. Res.* 41, W06013.
- Zhou, B., Greenhalgh, S.A., 2000. Cross-hole resistivity tomography using different electrode configurations. *Geophys. Pros.* 48, 887–912.